Available online at www.sciencedirect.com

ScienceDirect

Powder Technology 181 (2008) 292–300

POWDER TECHNOLOGY

www.elsevier.com/locate/powtec

Distinguishing between aggregates and agglomerates of flame-made TiO_2 by high-pressure dispersion

A. Teleki [a], R. Wengeler [b], L. Wengeler [a,c], H. Nirschl [b], S.E. Pratsinis [a,*]

[a] *Particle Technology Laboratory, Institute of Process Engineering, Department of Mechanical and Process Engineering, ETH Zurich, Sonneggstrasse 3 ML2 F13, CH-8092 Zurich, Switzerland*

[b] *Institute for Mechanical Process Engineering and Mechanics, Universität Karlsruhe (TH), D-76128 Karlsruhe, Germany*

[c] *Rheinisch-Westfälische Technische Hochschule Aachen, Aachen, Germany*

Received 9 May 2007; accepted 17 May 2007
Available online 24 May 2007

Abstract

The potential of high-pressure dispersion (HPD) and dynamic light scattering (DLS) is explored for rapid and quantitative estimation of the extent of particle aggregation and agglomeration by analyzing the entire particle size distribution. Commercially available and tailor-made TiO_2 particles by flame spray pyrolysis (FSP) were characterized by X-ray diffraction, nitrogen adsorption and transmission electron microscopy (TEM). Volume distributions of these titania particles were obtained by DLS of their electrostatically stabilized (with $Na_4P_2O_7$) aqueous suspensions. Dispersing these suspensions through a nozzle at 200 to 1400 bar reduced the size of agglomerates (particles bonded by weak physical forces) resulting in bimodal size distributions composed of their constituent primary particles and aggregates (particles bonded by strong chemical or sinter forces). Sintering FSP-made particles from 200 to 800 °C for 4 h progressively increased the minimum primary particle size (by grain growth) and aggregate size (by neck growth and phase transformation).

Keywords: Titanium dioxide; Aggregates; Agglomerates; Dispersion; Sintering; Dynamic light scattering

1. Introduction

Non-agglomerated TiO_2 particles are desired for pigments or composites [1] while agglomerated ones are desired when making catalyst pellets to facilitate reactant/product flow [2]. The interparticle bond energies can range from weak van der Waals forces (soft agglomerates or just agglomerates) to stronger solid-state necks (hard agglomerates or aggregates) [3]. Grass et al. [4] showed theoretically that in high-temperature synthesis of TiO_2, aggregate formation starts at the end of full coalescence and stops at the end of sintering where agglomerate formation starts. Though there are a number of techniques to measure agglomerate size there is rather little in discerning the degree of agglomeration quantitatively. For example, optical or electrical mobility techniques measure agglomerate sizes but nothing can be said if these are aggregates or agglomerates. Small angle scattering has been used to measure primary particle and aggregate sizes [5] and recently, even to monitor real-time agglomerate growth [6]. This is however a cumbersome technique with limited accessibility that is confined to fundamental studies rather than process instruments. Fragmentation of aerosols by impaction can give an estimate of the bond strength [7].

In post-synthesis processes, agglomerates can be ruptured by simple mechanical stirring, low-energy agitation [8] or ultrasonication [9]. However, for nanoparticles often higher stresses are needed to break even physical bonds, e.g., by ball milling [10] or high shear mixing in rotor–stator systems [11]. Particles are often contaminated from milling media and even phase transformation can be induced [12]. Ultrasonication initially breaks up agglomerates but later on leads to re-agglomeration [13]. High-pressure dispersion (HPD) of nanoparticle suspensions can lead to impurity-free fragmentation and minimize re-agglomeration [14]. This has been used to break flame-made agglomerates of SiO_2 nanoparticles. Physical bonding within agglomerates could be broken-up in turbulent flow resulting in

* Corresponding author. Tel.: +41 44 632 31 80; fax:+41 44 632 15 95.
E-mail address: pratsinis@ptl.mavt.ethz.ch (S.E. Pratsinis).

0032-5910/$ - see front matter © 2007 Elsevier B.V. All rights reserved.
doi:10.1016/j.powtec.2007.05.016

stable dispersions as was monitored by the diffusion equivalent particle diameter obtained from dynamic light scattering (DLS). Agglomerates in turbulent flow dissociate by break-up or erosion where primary particles are sheared from the agglomerate surface. Erosion and break-up can be distinguished by analysis of the fragment particle size distribution, as erosion yields a bimodal distribution by creating a distinct fine particle mode whereas simple break-up shifts the original mode to finer sizes [9].

Here the capacity of HPD for quantitative assessment of the fraction of single primary particles, aggregates and agglomerates is investigated, for the first time to the best of our knowledge, by examining the effect of applied pressure drop on the *entire* size distribution of flame-made TiO_2 particles. Upon dispersion of their suspension by HDP, the resulting fragment size distributions are analyzed by DLS as well as by nitrogen adsorption and X-ray diffraction monitoring thus both grain, crystallite and aggregate growth. Titania particles made by flame spray pyrolysis (FSP) [15] with closely controlled characteristics [16] as well as commercially available ones (Degussa P25) are characterized by HPD-DLS at various pressure drops obtaining the minimum fraction of unagglomerated particles. Furthermore, the degree of aggregation is increased progressively by sintering FSP-made TiO_2 particles at 200–800 °C for 4 h. These particles are characterized similarly to reveal primary particle growth, and most importantly, aggregate growth as a function of sintering temperature distinguishing between neck growth and phase transformation growth.

2. Experimental

2.1. Flame synthesis and sintering

The flame spray pyrolysis (FSP) reactor used for TiO_2 synthesis has been described in detail elsewhere [16]. Titanium-tetra-iso-propoxide (TTIP, Sigma-Aldrich, purity >97%) was used as precursor and diluted with xylene (Riedel-de-Haen) to a 0.8 M solution that was injected through the center capillary of the FSP nozzle by a syringe pump (Inotec, RS 232) at 5 ml/min. Oxygen (Pan Gas, purity >99%) was fed at 5 l/min through the surrounding annulus dispersing the solution into droplets. The pressure drop at the nozzle was held constant at 1.5 bar by adjusting the annulus gap width. A supporting premixed CH_4/O_2 (ratio: 1.5/3.2) flame surrounding the dispersion oxygen annulus ignited and stabilized the spray flame. A sinter metal ring surrounding the CH_4/O_2 flame supplied additional 5 l/min O_2-sheath. As reference, vapor-fed flame-made TiO_2 by Degussa (P25) was used (SSA = 50 m^2/g, d_{BET} = 30 nm, x_a = 34 nm, 82 wt.% anatase).

Product particles were sintered in a tubular oven (Nabertherm) for 4 h from 200 to 800 °C. The oven temperature was measured by a NiCr-Ni thermocouple (MDW GmbH, Type K) positioned right above the powder sample. The sample was placed on a metal sled and introduced into the pre-heated oven.

2.2. High-pressure dispersion

"As-prepared" TiO_2 particles (0.01 vol.% if not otherwise stated) were stirred into a solution of 0.1 mM $Na_4P_2O_7$ in distilled water for 10 min using a magnetic stirrer to ensure complete wetting. These suspensions were passed through a high-pressure dispersion apparatus described in detail elsewhere [14]. A pressure drop ranging from 200 to 1400 bar was applied by the high-pressure intensifier using pressurized air. The TiO_2 suspension was expanded through a 1 cm long nozzle of 125 μm diameter and collected for analysis in a container.

2.3. Particle and dispersion characterization

The specific surface area (SSA) was measured by nitrogen adsorption by a five-point Brunauer–Emmet–Teller method at 77K (Micrometrics Tristar 3000). The powder was dried by flowing nitrogen at 150 °C for at least 1 h prior to measurement. The BET-equivalent average diameter (d_{BET}) was calculated as $d_{BET} = 6/(SSA^*\rho_p)$, where ρ_p is the weighted density of TiO_2 (4260 or 3840 kg/m^3 for rutile or anatase, respectively). X-ray diffraction (XRD) patterns of the powders at $2\theta = 20-70°$ were obtained with a Bruker AXS D8 Advance diffractometer operating with Cu K_α radiation (40 kV, 40 mA). The fundamental parameter approach and the Rietveld method [17] were applied to determine the anatase and rutile crystallite sizes, x_a and x_r, respectively, and phase composition. Particle images were obtained by transmission electron microscopy (TEM; CM30ST microscope, FEI (Eindhoven), LaB6 cathode, operated at 300 kV, SuperTwin lens, point resolution ~2 Å). For TEM analysis the powders were mixed with ethanol and deposited onto a holey carbon foil supported on a copper grid. The suspensions were highly diluted with $Na_4P_2O_7$ solution and dropped onto carbon coated copper grids for TEM analysis (CM12, Philips) of the agglomerates before and after dispersion.

The zeta potential of the suspensions was measured with a Pen Kem 501 instrument (Collotec Messtechnik GmbH). Particle diameters in suspension were determined by dynamic light scattering (DLS, Beckmann Coulter, N4 Plus). An autocorrelation function was applied to calculate diffusion equivalent particle diameters (d_a) based on the Stokes–Einstein equation [14]. Particle volume distributions were calculated by a CONTIN algorithm [18,19].

2.4. Validation with SiO_2 agglomerates

The volume distributions obtained by DLS were compared to volume distributions obtained from SAXS and scanning mobility particle sizer (SMPS) measurements for vapor flame-made SiO_2 synthesized with 2 l/min O_2 and dispersed at Δp = 800 bar [14]. SAXS measurements were performed at the European Synchrotron Radiation Facility (Grenoble, FR) using the high brilliance SAXS beamline ID02. Data treatment and experimental setup are detailed in Wengeler et al. [14]. The volume distributions were obtained by fitting the scattering curve with a maximum entropy method [20] using a program developed by Jemian et al. [21].

For the SMPS measurements SiO_2 particles were dispersed without addition of stabilizer. An aerosol was prepared by passing the suspension through a Collison nebulizer [22] followed by a silica-gel diffusion dryer. The aerosol was then classified with a

differential mobility analyzer (DMA; Model Grimm 5.4–900 [23]) to obtain singly charged aerosol particles with a narrow size distribution. To further increase monodispersity, the small fraction of larger particles with multiple charges always present in DMA classified aerosols was removed with an impactor positioned upstream of the DMA. An aerosol stream with a constant flow rate of 0.3 l/min was drawn into a condensation particle counter (CPC; Model Grimm 5.403 [23]) using its internal pump. The particle number concentration was always $<10^4$ cm^{-3} so that only the more accurate, single particle count mode [23] of the CPC was used. The SMPS analysis could not be performed with TiO_2, as the particle suspensions are not stable without the addition of the stabilizer that crystallizes during drying and thus TiO_2 particle size distributions before/after dispersion cannot be measured.

Fig. 1 shows the volume distributions of flame-made SiO_2 obtained by DLS (circles), SAXS (triangles) and SMPS (squares). All measurements yielded distributions with two distinct peaks. The position of these was in good agreement, especially for DLS and SAXS as both are measured in the liquid phase. For SMPS measuring a silica aerosol, a broader distribution to smaller particle sizes is obtained, which might stem from nebulization and drying of the dispersion. In general, the largest error by DLS is caused by very broad distributions present in the sample. This mainly stems from the 6th power dependence of the radius to the scattered light.

3. Results and discussion

3.1. Particle synthesis and sintering characterization

Fig. 2 shows TEM images of the "as-prepared" (A) TiO_2 particles and after their sintering for 4 h at 400 (B), 600 (C) and 800 °C (D). Sinter necks cannot be discerned in the "as-prepared" sample, as well as for those sintered at 400 °C. In contrast, some necking appears at 600 °C that becomes dominant at 800 °C when particles have grown significantly and large sinter necks have evolved. Spherical particles are no longer visible. The sintering process is also depicted by the electron diffraction patterns (Fig. 2: insets): their intensity increases with sintering temperature so at 800 °C the pattern resembles that of single crystals.

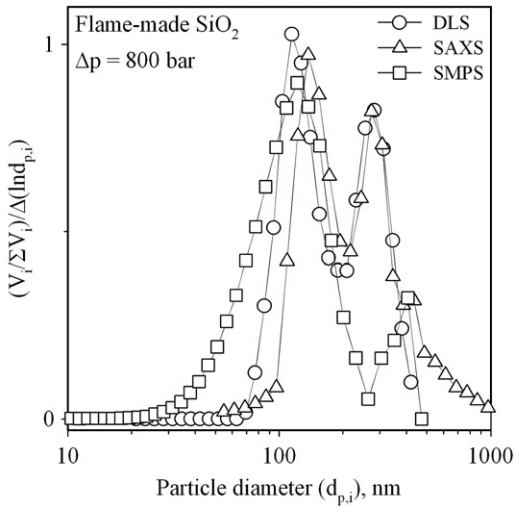

Fig. 1. Volume distributions for flame-made SiO_2 dispersed at 800 bar (2 l/min O_2) by DLS (circles), SAXS (triangles) and SMPS (squares).

Fig. 3 shows BET-equivalent particle diameter (circles), crystallite size (triangles) and anatase content (squares) as a function of sintering temperature for 4 h. The anatase content of the "as-prepared" powder is about 87 wt.%, typical for TiO_2 aerosol formation in rapidly cooled oxygen-rich flames [16,24]. The "as-prepared" anatase and rutile crystal sizes are about 24 and 11 nm, respectively, while the $d_{BET}=19$ nm. The anatase crystal size is larger than d_{BET}, indicating non-spherical, monocrystalline particles with little degree of aggregation as confirmed by TEM (Fig. 2A).

The anatase content is constant up to 400 °C while at 600 °C it has decreased slightly to 82 wt.%. At 800 °C a complete anatase to rutile transformation has taken place as expected at these temperatures [25] where d_{BET} and x_r also increase significantly to about 150 and 105 nm, respectively, in agreement with TEM (Fig. 2D). The d_{BET}, x_a and x_r had increased continuously, albeit slowly, below 600 °C. For example, d_{BET} increases from 19 nm for "as-prepared" particles to 27 nm when sintered at 600 °C. The enlargement of anatase crystallites with sintering temperature was also shown by Song and Pratsinis [25] who reported a steep increase in x_a of about 15 nm between 500 and 600 °C while here only an increase of about 3 nm is observed (Fig. 3). Their faster sintering rate of anatase crystals [25] might stem from the smaller starting crystallite size (about 10 nm) compared to the present study (Fig. 3). High SSA particles sinter and undergo phase transformation faster than low SSA ones [26,27]. This could be a result of more surface defects on high-area particles [26].

The d_{BET} increases during sintering with the evolution of sintering necks and coalescence of particles. This process starts at about 300 °C or even lower, whereas phase transformation sets in above 400 °C. Xia et al. [28] reported on a transformation temperature of 650 °C for 17 nm TiO_2 particles in good agreement with the data shown in Fig. 3. It was proposed by Amores et al. [29] that at the initial sintering stages the smallest particles with the highest defect densities coalesce forming larger anatase particles. Rutile then nucleates at the boundary of two anatase particles during their sintering and transforms into a larger particle [29], which would explain the large increase in rutile crystallite size at the transformation temperature (Fig. 3).

3.2. Particle dispersion

The zeta potential (ζ) of a suspension is a function of particle surface charge [30]. In dispersions where ζ is close to zero (isoelectric point), particles tend to agglomerate. At highly negative or positive ζ ($|\zeta|>30$ mV), particles in dispersions tend to repel each other and therefore do not agglomerate. The stabilizer $Na_4P_2O_7$ is a small, highly charged molecule with $P_2O_7^{4-}$ ions adsorbing to the particle surface. As ζ increases, the suspension is electrostatically stabilized, e.g., the steric contribution to the stabilization is small [31]. Fig. 4 shows zeta potential (filled symbols, left axis) and mean hydrodynamic particle diameters d_a (open symbols, right axis) obtained by DLS of TiO_2 Degussa P25 (circles) and "as-prepared" here by FSP (squares) as a function of

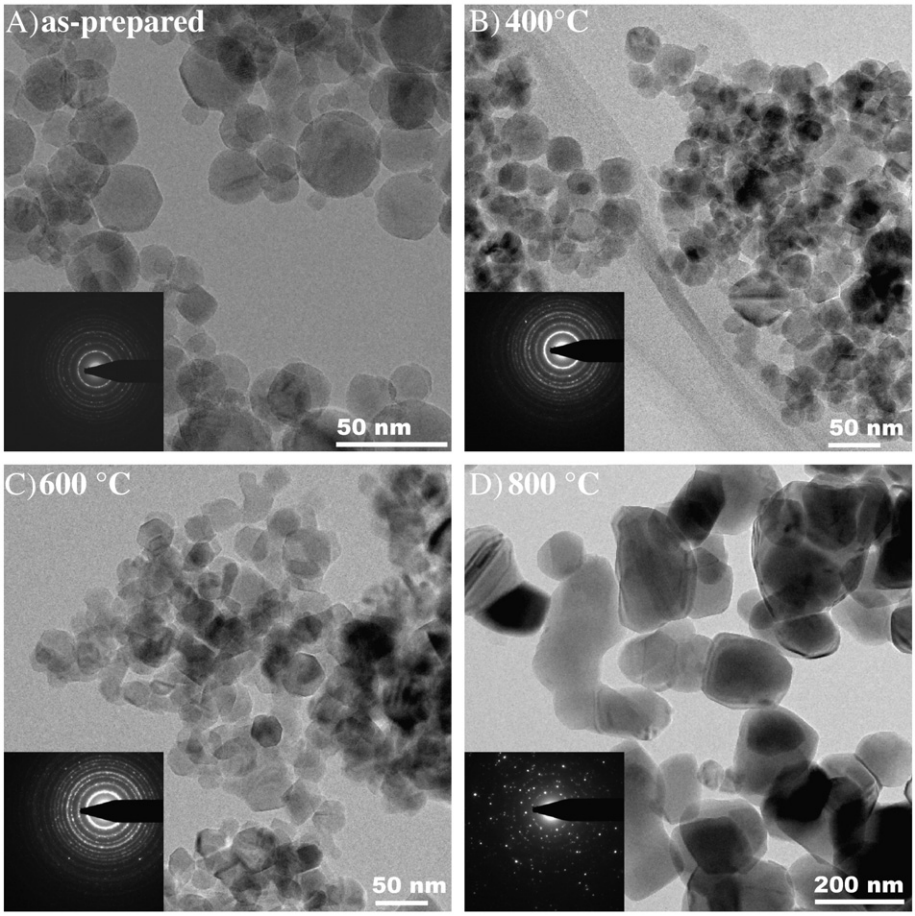

Fig. 2. TEM images of the "as-prepared" FSP-made TiO_2 (A), as well as sintered at 400 (B), 600 (C) and 800 °C (D).

$Na_4P_2O_7$ concentration. As the zeta potential measurements could only be conducted in a very narrow particle concentration range due to instrument limitations, a particle concentration of 0.005 vol.% was chosen. However, a significant (10%) deviation of ζ at increased particle volume concentrations was shown previously only for 0.001 mM $Na_4P_2O_7$ at higher concentrations (0.1 vol.% for P25). Thus the ζ measured here should be comparable to the ones during dispersion (0.01 particle vol.%).

Without stabilization, large flocs are formed and particle size as well as zeta potential cannot be measured (Fig. 4). At 0.001 mM $Na_4P_2O_7$ the zeta potential of P25 (filled circles) is

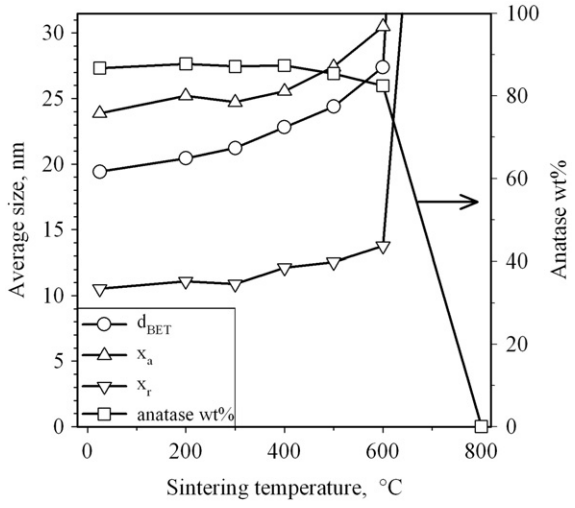

Fig. 3. BET-equivalent TiO_2 particle diameter (circles), anatase (up-triangles) and rutile (down-triangles) crystallite sizes, and anatase weight fraction (squares, right axis) as a function of sintering temperature.

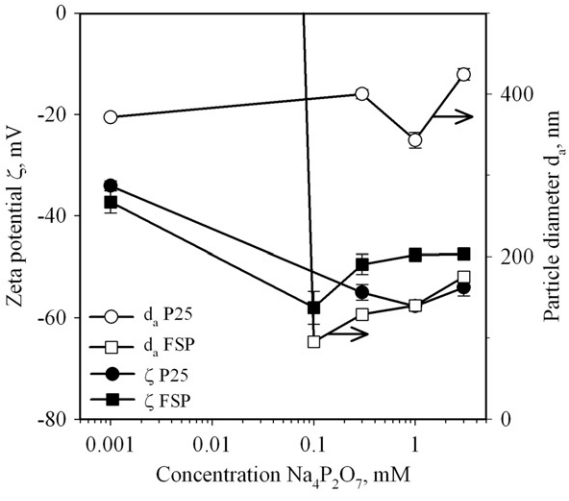

Fig. 4. Zeta potential (filled symbols) and particle diameters (open symbols) of Degussa P25 (circles) and FSP-made TiO_2 (squares) as a function of $Na_4P_2O_7$ concentration in the solution. The particle concentration in solution was 0.005 vol.%.

−34 mV, this decreases to −55 mV at 0.3 mM $Na_4P_2O_7$. Increasing the $Na_4P_2O_7$ concentration above 1 mM, slightly increases ζ. The P25 particle diameter (open circles) of about 400 nm was not largely influenced by the $Na_4P_2O_7$ concentration. For the FSP sample the most stable suspension was found at a $Na_4P_2O_7$ concentration of 0.1 mM (ζ=−58 mV, filled squares). At this concentration the particle diameter was 96 nm (open squares), while initially at 0.001 mM $Na_4P_2O_7$ a very large particle diameter was measured (~8000 nm). The particle diameter then increased as the $Na_4P_2O_7$ concentration was increased and the solution became more unstable. Based on these results, a $Na_4P_2O_7$ concentration of 0.1 mM was chosen to assure stable suspensions. The particle sizes of selected samples were re-measured after 2 weeks storage and no changes were detected, thus demonstrating the long-term suspension stability.

3.3. Agglomerate fragmentation

During high-pressure dispersion, Reynolds stresses arising from turbulent flow velocity fluctuations break up agglomerate structures by shear and elongation in turbulent eddies [14]. This is demonstrated here by the shift of the particle volume distribution of the "as-prepared" TiO_2 to smaller sizes with increasing dispersion pressure drop (Fig. 5A). Initially (0 bar, circles) a unimodal distribution peaking at 70 nm is obtained and its large tail reaches up to 340 nm. After dispersion at 200 bar (up-triangles), the large tail of the distribution has shifted substantially to smaller sizes with the smallest reaching 30 nm, indicating break-up of these large agglomerates. After dispersion at 800 bar (squares) the peak is still around 70 nm though, a distinct second peak appears at 30 nm now. This becomes even more evident after dispersion at 1200 (down-triangles) and 1400 bar (diamonds) where a bimodal distribution is observed with a peak of high intensity at 25 nm and a second smaller mode at about 70 nm.

The size of the first peak is comparable to the primary particle size (Fig. 2) indicating that this mode consists mostly of single primary particles. The bimodal distribution obtained after dispersion at 1200 and 1400 bar becomes even more evident in the cumulative representation of the volume distributions (Fig. 5B). It also shows that the larger mode of the distribution is no longer shifted at pressure drops >800 bar indicating that it consists mostly of aggregates. Furthermore Fig. 5B shows that the fine mode that represents at least 45% of the total mass (at 1400 bar) consists mostly of non-aggregated primary particles of similar size to the BET and XRD sizes.

After dispersion at 1400 bar agglomerates were broken up into their constituent primary particles (peak around 25 nm) and aggregates (peak around 70 nm). This is shown in TEM images of Fig. 6 of the "as-prepared" (0 bar, A) and dispersed at 1400 bar sample (B). In the "as-prepared" sample large agglomerate structures can be seen. The smaller agglomerates are aggregates as structures of similar size can still be found after dispersion at 1400 bar. At 1400 bar also small clusters of primary particles are visible, in agreement with the small mode in the measured distribution (Fig. 5A). Similarly by ultrasonication, after a rapid initial size reduction, continued ultrasonication does not further

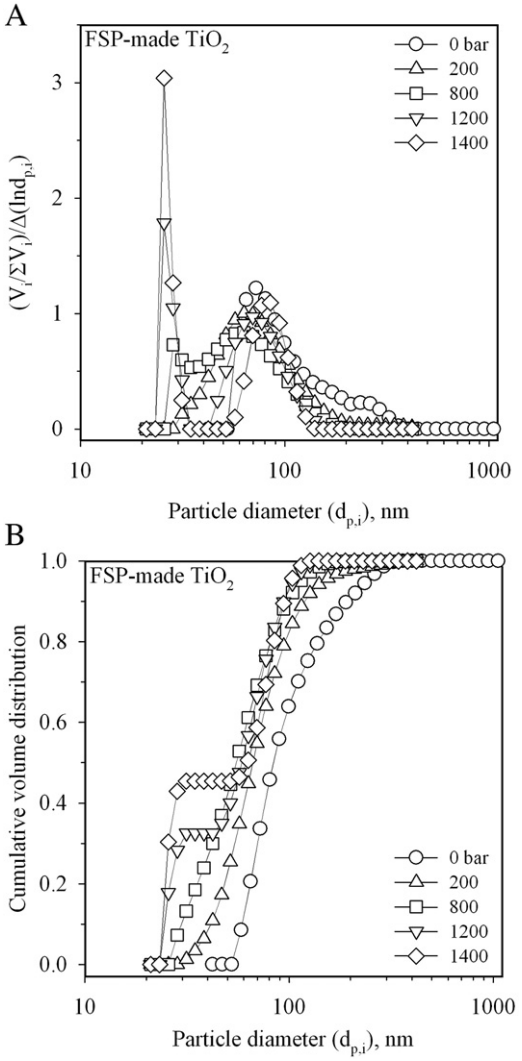

Fig. 5. Volume (A) and cumulative (B) distribution of "as-prepared" FSP-made TiO_2 particles after dispersion at different pressure drops.

alter the size significantly [13,32] and nanopowders cannot be broken completely down to their primary particle size [30]. This is attributed to erosion mechanism where primary particles and small aggregates consisting of a few primary particles break away from the larger agglomerates [30] as with ultrasonication of sol–gel made silica agglomerates also [9]. Also during impaction of aerosol agglomerates only bonds between clusters are broken while the subunits themselves do not fragment [7].

The volume distributions of Degussa's P25 TiO_2 after dispersion are shown in Fig. 7A. Initially (0 bar, circles) the distribution is unimodal with a peak at 400 nm. As the P25 suspension is dispersed, bimodal distributions are obtained at all applied pressure drops. After dispersion at 200 bar the small and large particle modes are located at 70 and 280 nm, respectively. With increasing pressure drop both peaks are shifted to smaller sizes and the intensity of the large particle mode decreases while that of the small mode increases. At 1400 bar (diamonds) the small and large particle modes have shifted to about 50 and 200 nm, respectively. Mandzy et al. [30] measured initial agglomerate sizes of 1 μm for Degussa P25 in aqueous (pH=8)

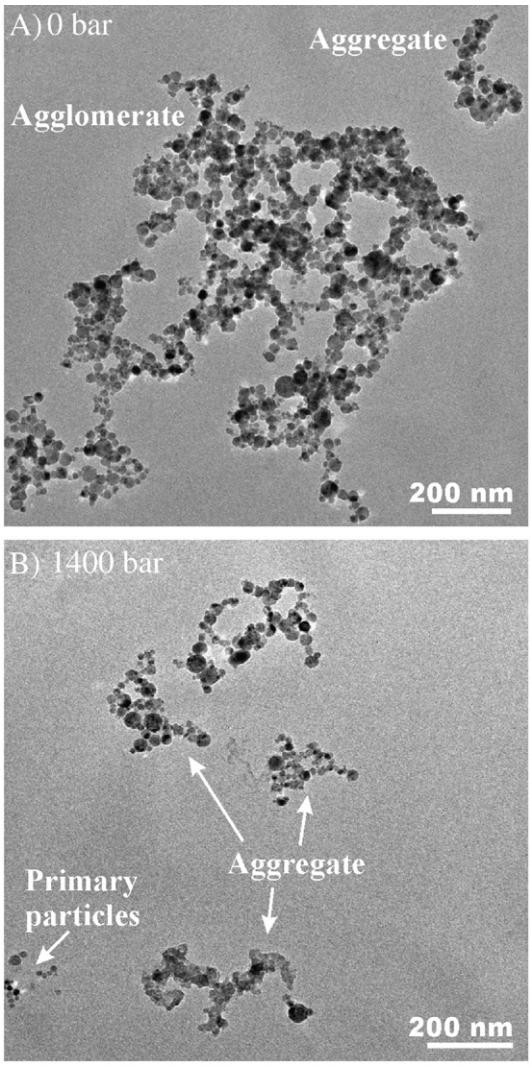

Fig. 6. TEM images of FSP particles "as-prepared" (A) and after dispersion at 1400 bar (B).

solutions, this was reduced to about 200 nm after ultrasonication (24 kHz) for 2 h, in agreement with the large particle mode obtained here after dispersion at 1400 bar (Fig. 7). They also showed a second mode <100 nm of very low intensity after ultrasonication which did not coincide with the primary particle size.

This indicates that the large P25 mode is constituted initially of aggregates and agglomerates that are broken at 1400 bar down to constituent smaller aggregates and few, if any, primary particles as the fine particle mode is larger than the P25 primary particle diameter of d_{BET}=30 nm. In contrast, at the same dispersion pressure, the fine mode of FSP-made TiO_2 was rather close to its primary particle diameter of d_{BET}=20 nm (Fig. 5A, diamonds). Also, a bimodal fragment distribution was obtained already at 200 bar dispersion for P25 (Fig. 7B) in contrast to that obtained at 1200 bar for FSP TiO_2 (Fig. 5B). The small mode in P25 is shifted to smaller sizes as the pressure drop increases (Fig. 7B), most likely by erosion from larger agglomerates as the mass of fines is increasing (Fig. 7B). The fine particle mode of FSP-made TiO_2 was increased as the dispersion pressure drop was increased from 1200 to 1400 bar but did not shift to smaller sizes (Fig. 5B). As the fine mode of P25 TiO_2 is larger than its d_{BET} and d_{XRD} even at 1400 bar, it can be concluded it has few, if any, non-aggregated particles in contrast to FSP-made TiO_2 that contained, at least, 45% of them in non-aggregated state at the same conditions.

3.4. Influence of sintering temperature on aggregate size

As FSP-made particles are rather non-aggregated, their extent of aggregation can be increased by controlled sintering. Fig. 8 shows volume distributions of FSP-made TiO_2 sintered in air at 200 (A), 400 (B), 600 (C) and 800 °C (D) for 4 h and dispersed at different Δp. Initially after sintering at 200 °C (Fig. 8A, circles) a bimodal distribution is observed with peaks at 110 and 250 nm with a large tail reaching up to 500 nm. After dispersion at 200 bar the small peak shifts to 70 nm while the largest one disappears (Fig. 8A, triangles). The intensity of the large tail decreases but a higher fraction of particles >100 nm is

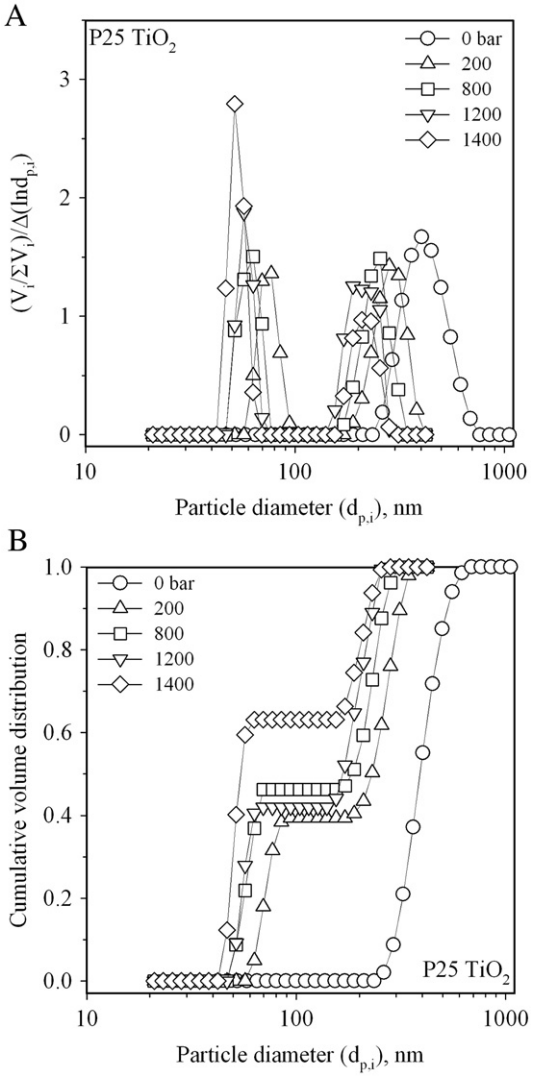

Fig. 7. Volume (A) and cumulative (B) distribution of P25 particles after dispersion at different pressure drops.

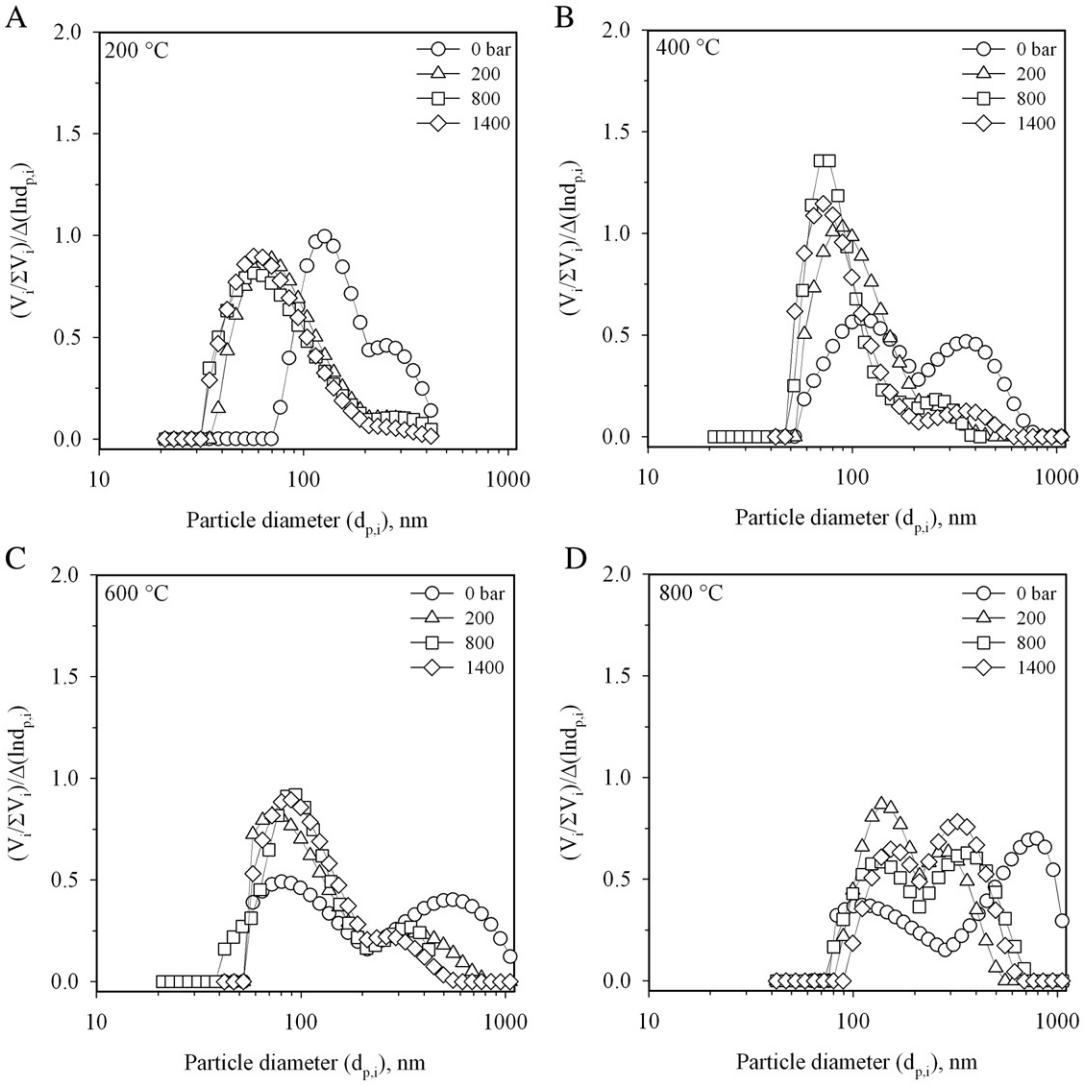

Fig. 8. Volume distribution of FSP-made particles that had been sintered at 200 (A), 400 (B), 600 (C) and 800 °C (D) for 4 h prior to dispersion at the indicated pressure drops.

still present compared to the "as-prepared" sample dispersed at 200 bar (Fig. 5A, triangles). The peak shifts to 60 nm after dispersion at 1400 bar, however a bimodal distribution is not obtained as was observed for the "as-prepared" FSP sample (Fig. 5A, diamonds). A mode equivalent to the primary particle size is not obtained.

Clearly even this gentle sintering increased the strength of bonding especially between the smallest particles. No particles smaller than 35 nm are found in Fig. 8A in contrast to 30 nm in Fig. 5A at the same dispersion pressure. Interestingly enough the large tail of the PSD is similar to that of 1400 bar in Fig. 5A indicating that sintering at 200 °C had little, if any, effect on large particles.

After sintering at 400 °C initially the distribution has two distinct peaks at 120 and 350 nm with a tail of the distribution reaching up to particle diameters of nearly 700 nm (Fig. 8B, circles). The large mode is shifted to 250 nm and reduced significantly in intensity by dispersion at 200 bar as the agglomerates are broken-up (Fig. 8B, triangles). The small mode is only slightly shifted to 70 nm by dispersion at 800 bar (Fig. 8B, squares) and is not further altered at 1400 bar (diamonds). The slight movement of the PSD by dispersion towards smaller sizes means that larger aggregates have been formed upon sintering at 400 than at 200 °C. The fact that the fine particle mode has grown to 70 nm in diameter even after 1400 bar dispersion while grain and crystallite sizes remain in the "as-prepared" order of 20 nm (Fig. 3) indicates that only sinter necks have been formed by sintering at 400 °C that can be only detected by high-pressure dispersion and DLS.

After sintering at 600 °C (Fig. 8C) the distribution peaks at 80 and 500 nm. Upon dispersion, the large peak is reduced while the small remains intact regardless of the employed pressure drop. This indicates that the building blocks of agglomerates are aggregates of about 80-nm diameter on the average. Initially the large tail of the distribution is reaching up to agglomerate diameters of larger than 1 μm. Its intensity decreases and shifts the peak to smaller sizes with increasing dispersion pressure that breaks these agglomerates. Some,

however, are still present even after dispersion at 1400 bar. This indicates further that hard sinter bonds have been developed holding these particles together even after dispersion at 1400 bar. Again the primary particle characteristics remain in the order of 20 nm (Fig. 3) while the smallest DLS particle size is 50 nm further proving the formation of polycrystalline, TiO_2 aggregates by sintering.

After sintering at 800 °C (Fig. 8D, circles) bimodally distributed agglomerates, even larger than 1 μm, are present. These were observed also during stirring the suspensions as large flocs readily sedimented and thus DLS measurements could not be performed with the same accuracy. As a result, the DLS measurement (Fig. 8D, circles) of the "as-prepared" particles is not reliable. These large flocs were broken up by dispersion at 200 bar (triangles) resulting in two peaks at 140 and 300 nm, respectively. The first mode corresponds rather closely to the primary particle size d_{BET} (150 nm) and to some extent to the rutile crystallite size x_r (105 nm; Fig. 3) indicating that it is constituted by rutile (in some cases even monocrystalline) particles. The distribution is hardly altered by dispersion at higher Δp, showing the high bond strength of aggregates even in the "large" size mode.

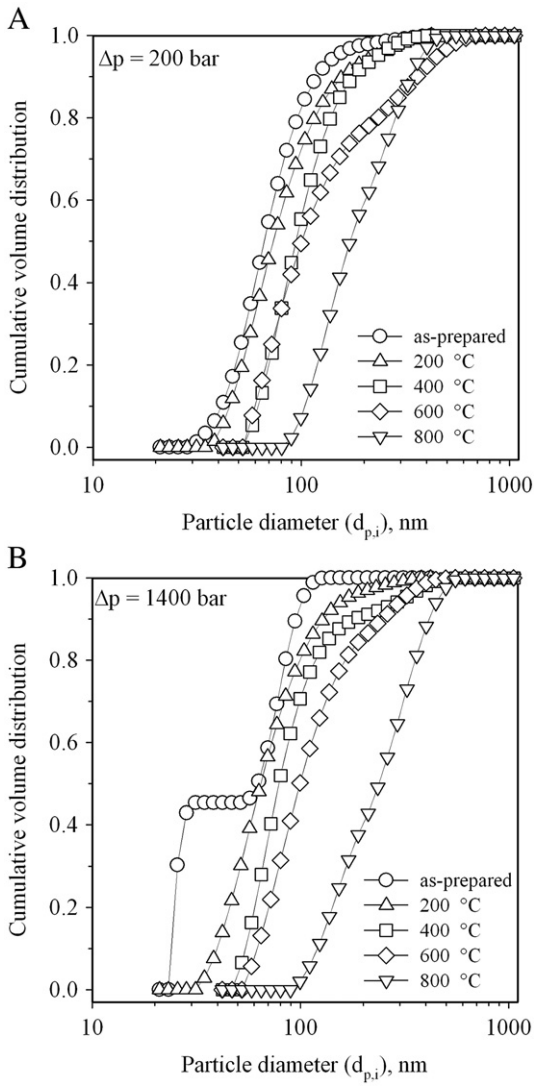

Fig. 9. Cumulative volume distribution of the "as-prepared" and sintered FSP-made particles after dispersion at 200 (A) and 1400 bar (B).

Fig. 9A shows the FSP-made TiO_2 particle cumulative volume distributions of the "as-prepared" (circles) and sintered at 200–800 °C after dispersion at 200 bar. The distributions are shifted towards larger sizes with increasing sintering temperature. The distributions at 400 and 600 °C are nearly identical while a large shift is seen after sintering at 800 °C. This is also the temperature where a nearly complete phase transformation from anatase to rutile has occurred (Fig. 3, squares).

Fig. 9B shows the volume cumulative distributions of the "as-prepared" and sintered FSP-made TiO_2 after dispersion at 1400 bar. The initial bimodal distribution is made of primary and aggregate particles as shown in Fig. 5B but quickly becomes unimodal upon sintering of the primary particle mode at 200 °C as shown in Fig. 8A (triangles). Again the aggregate diameters increase with increasing sintering temperature. After sintering at 200 °C more but not larger aggregates have been formed compared to the "as-prepared" sample since that temperature is not high enough to affect the extent of aggregation between large particles. The distributions of the samples sintered at 600 and 800 °C are nearly identical to the ones after 200 bar dispersion (Fig. 9A) as strong bonds between aggregates have been created that cannot be broken by HPD. As with dispersions at $\Delta p = 200$ bar, a large increase in aggregate particle diameter from 600 to 800 °C (Fig. 9B) is attributed to the anatase–rutile phase transformation (Fig. 3).

4. Conclusions

Dispersion of aqueous suspensions of flame-made TiO_2 particles at increasing pressure drop (up to 1400 bar) and dynamic light scattering was used to determine and quantify, for the first time, their extent of aggregation or agglomeration as a function of applied dispersion pressure. Upon dispersion, the peak of the FSP-made fine particle mode (45% of total mass) was comparable to its primary particle diameter and crystallite size. This indicates that, at least, 45% by mass of FSP-made TiO_2 is non-aggregated. In contrast, upon dispersion even the fine particle mode (60% of total mass) of P25 TiO_2 was distinctly larger than its BET and XRD particle size indicating that P25 is composed largely of aggregates. Controlled sintering of FSP-made TiO_2 from 200 to 800 °C for 4 h demonstrated further the capacity of high-pressure dispersion to assess the extent of particle aggregation. Increasing the sintering temperature resulted in larger fine particles even at the lowest temperatures (e.g. 200 °C) and enhanced the formation of aggregates by anatase to rutile phase transformation especially at the highest temperatures (e.g. 800 °C).

Acknowledgements

We thank Dr. Frank Krumeich at the Laboratory of Inorganic Chemistry, ETH Zurich (Switzerland) for the preparation of TEM images. Financial support by the Swiss National Science Foundation (No. 200020-112111/1), the German Science

Foundation (DFG; No. PAK 75/1) and the Ministry of Science, Research and the Arts "Baden-Württemberg" is gratefully acknowledged. This paper received the second Best Poster Award at PARTEC 2007, International Congress for Particle Technology, March 27–29, 2007, Nuremberg, Germany.

References

[1] R. Mueller, H.K. Kammler, S.E. Pratsinis, A. Vital, G. Beaucage, P. Burtscher, Non-agglomerated dry silica nanoparticles, Powder Technology 140 (1-2) (2004) 40–48.
[2] H.K. Kammler, L. Madler, S.E. Pratsinis, Flame synthesis of nanoparticles, Chemical Engineering and Technology 24 (6) (2001) 583–596.
[3] S. Tsantilis, S.E. Pratsinis, Soft- and hard-agglomerate aerosols made at high temperatures, Langmuir 20 (14) (2004) 5933–5939.
[4] R.N. Grass, S. Tsantilis, S.E. Pratsinis, Design of high-temperature, gas-phase synthesis of hard or soft TiO_2 agglomerates, AIChE Journal 52 (4) (2006) 1318–1325.
[5] J. Hyeon-Lee, G. Beaucage, S.E. Pratsinis, S. Vemury, Fractal analysis of flame-synthesized nanostructured silica and titania powders using small-angle X-ray scattering, Langmuir 14 (20) (1998) 5751–5756.
[6] H.K. Kammler, G. Beaucage, D.J. Kohls, N. Agashe, J. Ilavsky, Monitoring simultaneously the growth of nanoparticles and aggregates by in situ ultra-small-angle X-ray scattering, Journal of Applied Physics 97 (5) (2005) 054309.
[7] S. Froeschke, S. Kohler, A.P. Weber, G. Kasper, Impact fragmentation of nanoparticle agglomerates, Journal of Aerosol Science 34 (3) (2003) 275–287.
[8] C. Saltiel, Q. Chen, S. Manickavasagam, L.S. Schadler, R.W. Siegel, M.P. Menguc, Identification of the dispersion behavior of surface treated nanoscale powders, Journal of Nanoparticle Research 6 (1) (2004) 35–46.
[9] K.A. Kusters, S.E. Pratsinis, S.G. Thoma, D.M. Smith, Ultrasonic fragmentation of agglomerate powders, Chemical Engineering Science 48 (24) (1993) 4119–4127.
[10] D.F. Kelsall, P.S.B. Stewart, K.R. Weller, Continuous grinding in a small wet ball mill: 4. Study of influence of grinding media load and density, Powder Technology 7 (5) (1973) 293–301.
[11] M. Pohl, H. Schubert, H.P. Schuchmann, Production of stable dispersions from pyrogenic silicic acid, Chemie Ingenieur Technik 77 (3) (2005) 258–262.
[12] S. Sen, M.L. Ram, S. Roy, B.K. Sarkar, The structural transformation of anatase TiO_2 by high-energy vibrational ball milling, Journal of Materials Research 14 (3) (1999) 841–848.
[13] M. Aoki, T. Ring, J. Haggerty, Analysis and modeling of the ultrasonic dispersion technique, Advanced Ceramic Materials 2 (3A) (1987) 209–212.
[14] R. Wengeler, A. Teleki, M. Vetter, S.E. Pratsinis, H. Nirschl, High pressure liquid dispersion and fragmentation of flame-made silica agglomerates, Langmuir 22 (2006) 4928–4935.
[15] L. Madler, H.K. Kammler, R. Mueller, S.E. Pratsinis, Controlled synthesis of nanostructured particles by flame spray pyrolysis, Journal of Aerosol Science 33 (2) (2002) 369–389.
[16] H. Schulz, L. Madler, R. Strobel, R. Jossen, S.E. Pratsinis, T. Johannessen, Independent control of metal cluster and ceramic particle characteristics during one-step synthesis of Pt/TiO_2, Journal of Materials Research 20 (9) (2005) 2568–2577.
[17] R.W. Cheary, A.A. Coelho, Axial divergence in a conventional X-ray powder diffractometer: I. Theoretical foundations, Journal of Applied Crystallography 31 (1998) 851–861.
[18] S.W. Provencher, A constrained regularization method for inverting data represented by linear algebraic or integral-equations, Computer Physics Communications 27 (3) (1982) 213–227.
[19] S.W. Provencher, Contin — a general-purpose constrained regularization program for inverting noisy linear algebraic and integral-equations, Computer Physics Communications 27 (3) (1982) 229–242.
[20] J.A. Potton, G.J. Daniell, B.D. Rainford, Particle size distributions from SANS data using the maximum entropy method, Journal of Applied Crystallography 21 (1988) 663–668.
[21] P.R. Jemian, J.R. Weertman, G.G. Long, R.D. Spal, Characterization of 9Cr-1MoVNb steel by anomalous small-angle X-ray scattering, Acta Metallurgica et Materialia 39 (11) (1991) 2477–2487.
[22] K.R. May, The collison nebulizer: description, performance and application, Journal of Aerosol Science 4 (3) (1973) 235–243.
[23] M. Heim, G. Kasper, G.P. Reischl, C. Gerhart, Performance of a new commercial electrical mobility spectrometer, Aerosol Science and Technology 38 (2004) 3–14.
[24] A. Teleki, S.E. Pratsinis, K. Wegner, R. Jossen, F. Krumeich, Flame-coating of titania particles with silica, Journal of Materials Research 20 (5) (2005) 1336–1347.
[25] K.C. Song, S.E. Pratsinis, Synthesis of bimodally porous titania powders by hydrolysis of titanium tetraisopropoxide, Journal of Materials Research 15 (11) (2000) 2322–2329.
[26] G. Oliveri, G. Ramis, G. Busca, V.S. Escribano, Thermal-stability of vanadia-titania catalysts, Journal of Materials Chemistry 3 (12) (1993) 1239–1249.
[27] A.A. Gribb, J.F. Banfield, Particle size effects on transformation kinetics and phase stability in nanocrystalline TiO_2, American Mineralogist 82 (7–8) (1997) 717–728.
[28] B. Xia, H.Z. Huang, Y.C. Xie, Heat treatment on TiO_2 nanoparticles prepared by vapor-phase hydrolysis, Materials Science & Engineering. B, Solid-State Materials for Advanced Technology 57 (2) (1999) 150–154.
[29] J.M.G. Amores, V.S. Escribano, G. Busca, Anatase crystal-growth and phase-transformation to rutile in high-area TiO_2, MoO_3-TiO_2 and other TiO_2-supported oxide catalytic-systems, Journal of Materials Chemistry 5 (8) (1995) 1245–1249.
[30] N. Mandzy, E. Grulke, T. Druffel, Breakage of TiO_2 agglomerates in electrostatically stabilized aqueous dispersions, Powder Technology 160 (2) (2005) 121–126.
[31] R. Greenwood, K. Kendall, Selection of suitable dispersants for aqueous suspensions of zirconia and titania powders using acoustophoresis, Journal of the European Ceramic Society 19 (4) (1999) 479–488.
[32] O. Vasylkviv, Y. Sakka, Synthesis and colloidal processing of zirconia nanopowder, Journal of the American Ceramic Society 84 (11) (2001) 2489–2494.